Electronic Supplementary Material (ESI) for Dalton Transactions.

Supporting Information for:

Characterisation of intergrowth in metal oxide materials using structure-mining: the case of γ-MnO_2

Nicolas P. L. Magnard, Andy S. Anker, Olivia Aalling-Frederiksen, Andrea Kirsch and Kirsten M. Ø. Jensen*

*kirsten@chem.ku.dk

Department of Chemistry and Nano-Science Center, University of Copenhagen, 2100 Copenhagen Ø, Denmark

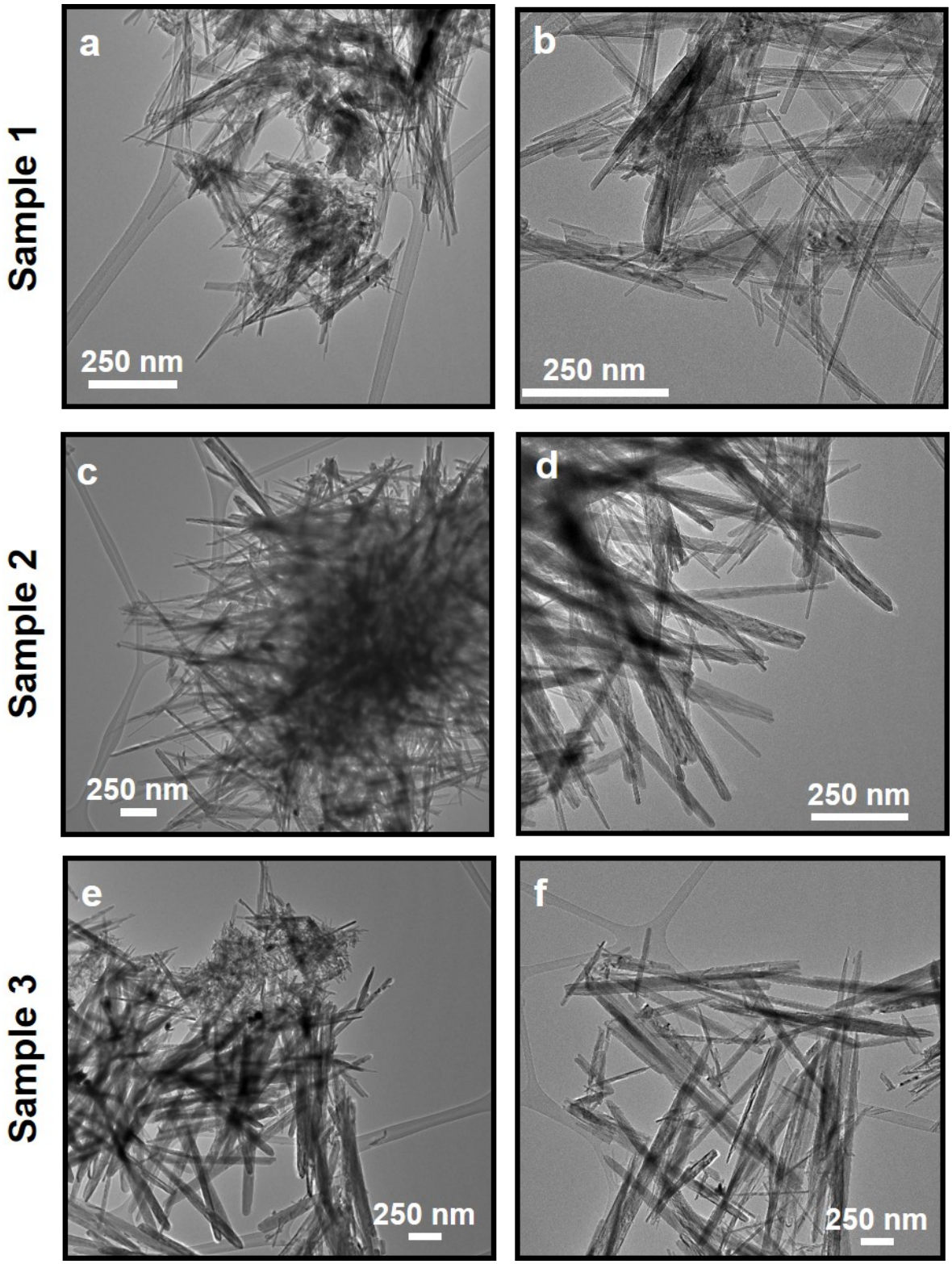

Figure S1: TEM images of sample 1(a-b), 2(c-d) and 3(e-f)

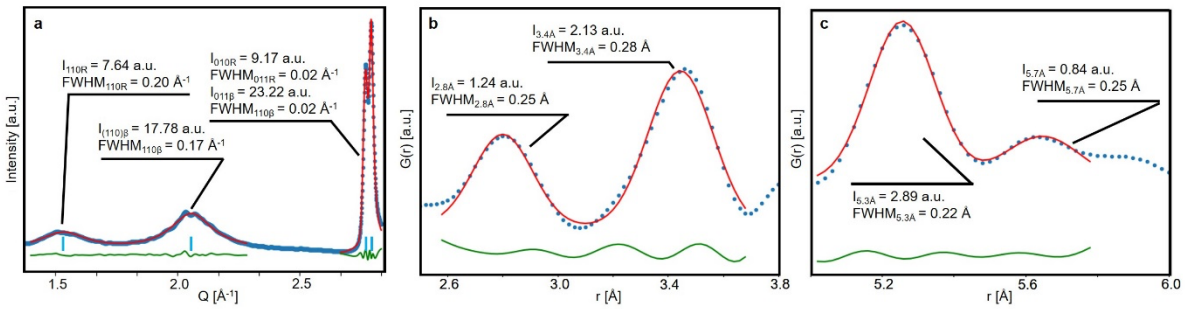

Figure S2: Example of fitting procedure of Bragg peaks on XRD data (a) and pair distance at 2.8 and 3.4 Å (b) and 5.3 and 5.7 Å (c) on PDF data. Here the peak fitting is performed on the calculated XRD pattern and PDF of the mined superstructure with P_b = 0.5 and P_r = 0.7. For Bragg peaks, a Pseudo-Voight function is fitted on the peak and for pair distance peak, a Gaussian function is used for the fit. For both, experimental data points are represented by blue dots, the calculated model by a solid red line and the difference curve by a solid green line.

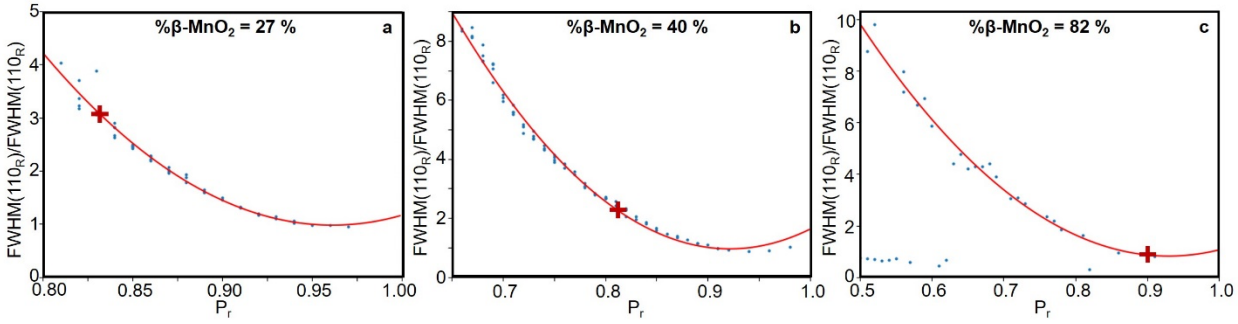

Figure S3: Ratio between the FWHM of the 110_R and 011_R lines from the modelled XRD patterns plotted against P_r (blue dots) fitted using a quadratic trend (red solid line) using patterns for which %β-MnO_2 = 27 % for sample 1 (a), %β-MnO_2 = 40 % for sample 2 (b), %β-MnO_2 = 82 % for sample 3 (c).

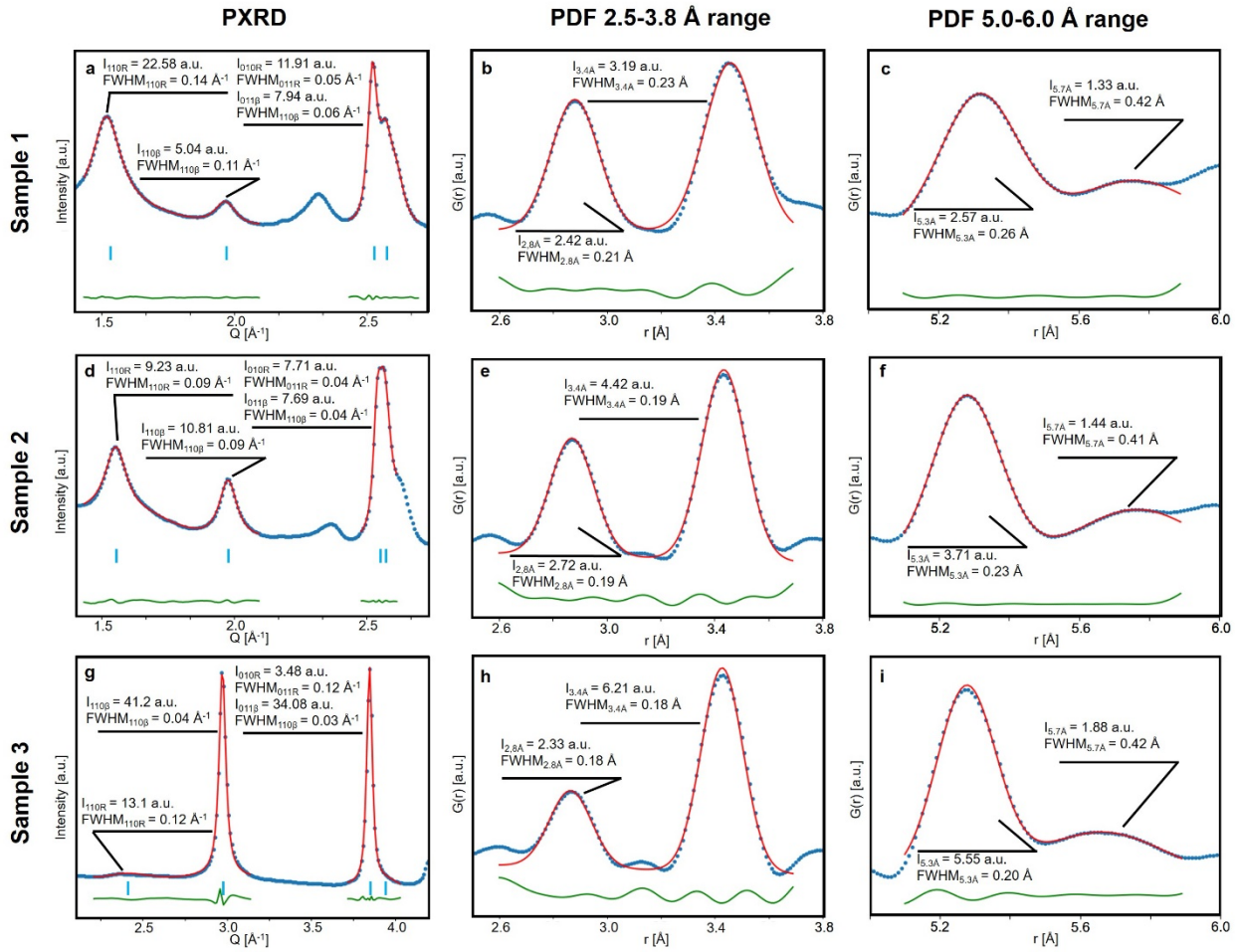

Figure S4: Fitting of the 110_R, 110_β, 011_R and 011_β Bragg peaks on XRD data (a, c, g) and pair distance at 2.8 and 3.4 Å (b, e, h) and 5.3 and 5.7 Å (c, f, i) on PDF data, of samples 1, 2 and 3. For Bragg peaks, a Pseudo-Voight function is fitted on the peak and for pair distance peak, a Gaussian function is used for the fit. For both, experimental data points are represented by blue dots, the calculated model by a solid red line and the difference curve by a solid green line.

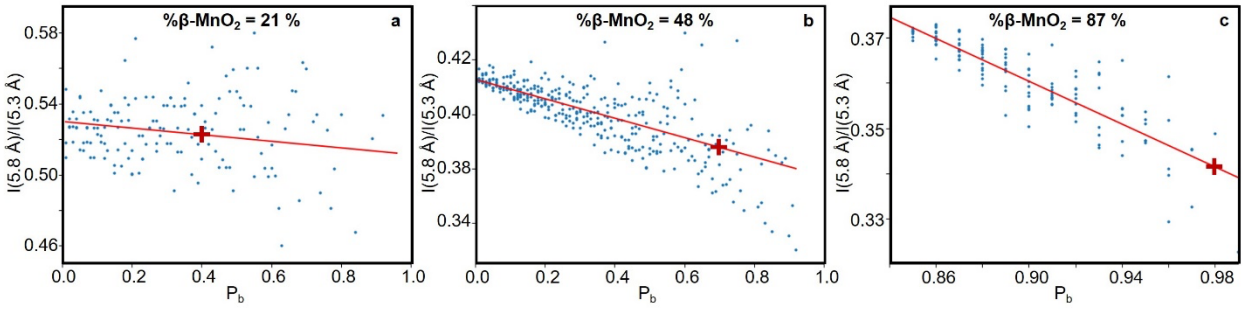

Figure S5: Ratio between the intensity of peaks at 5.3 and 5.8 Å from the modelled PDF patterns plotted against P_b (blue dots) fitted using a quadratic trend (red solid line) using patterns for which %β-MnO_2 = 27 % for sample 1 (a), %β-MnO_2 = 40 % for sample 2 (b), %β-MnO_2 = 82 % for sample 3 (c).

Refined parameter XRD	*Sample 2 superstructure (0.72, 0.81)*
a (Å)	1140.855
b (Å)	4.443
c (Å)	2.874
B_{iso} Mn (Å^2)	0.0843
B_{iso} O (Å^2)	0.1683

Refined parameter PDF	*Sample 2 superstructure (0.69, 0.72)*
a (Å)	1132.151
b (Å)	4.429
c (Å)	2.869
B_{iso} Mn (Å^2)	0.1594
B_{iso} O (Å^2)	0.2921

Table S1: Example of refined parameters during the structure-mining of sample 2 on XRD (a) and PDF (b). The refined superstructure whose results are shown here corresponds to the one for which the (Pr, Pb) couple is determined by the peak-fitting analysis, respectively (0.72, 0.81) for XRD and (0.69, 0.72) for PDF.

Sample	*P_b*	*P_r*	*Phase fraction of α-MnO_2 (%)*
Sample 1	0.53	0.87	12.5
Sample 2	0.69	0.72	18.1
Sample 3	0.97	0.9	12.8

Table S2: Refined volumetric phase fraction of α-MnO_2 by Rietveld refinement of superstructures with (P_b, P_r) couple found with the peak-fitting analysis on samples 1, 2 and 3.

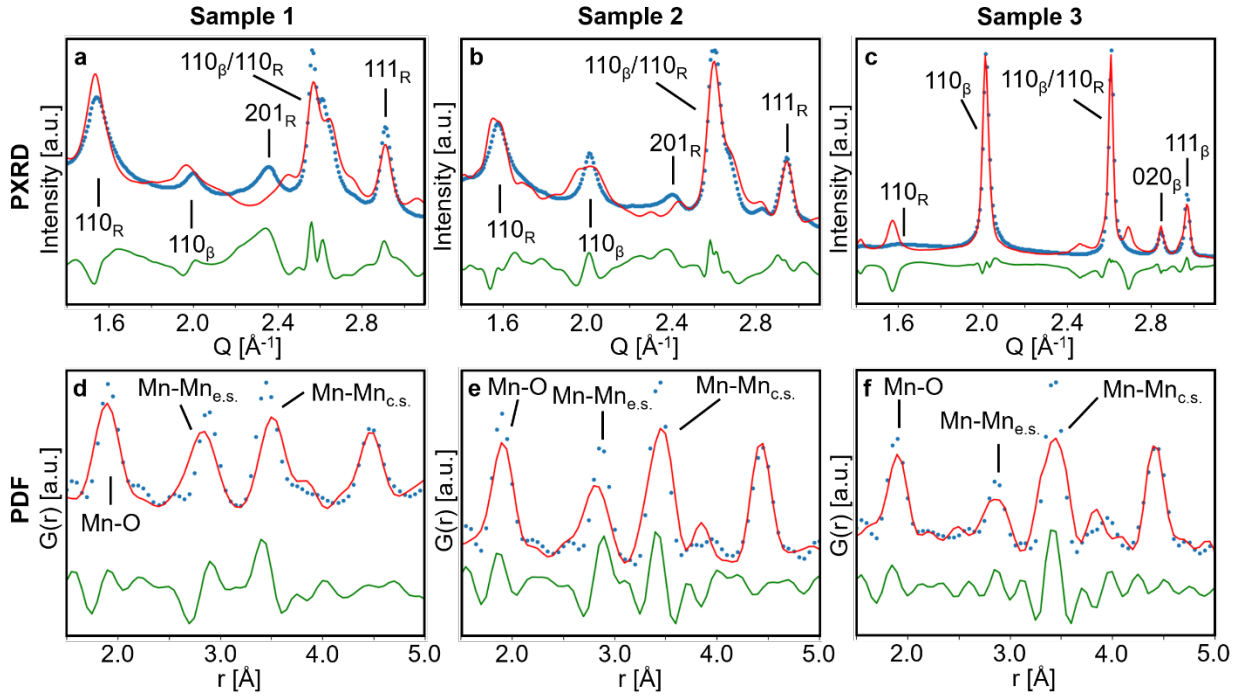

Figure S6: Enlargement of the low Q and low r region of the Rietveld and PDF refinements shown in Figure 6. Rietveld and PDF refinements of sample 1 are shown in (a, d), sample 2 in (b, e) and sample 3 in (c, f) respectively.

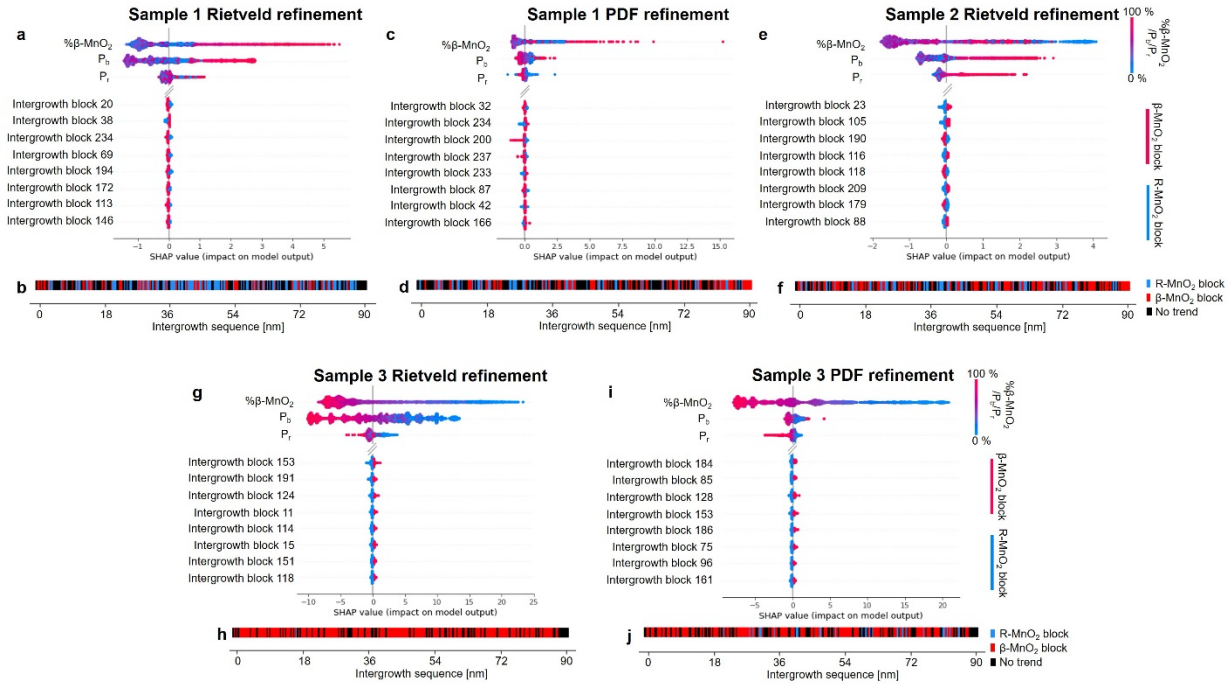

Fig S7: Summary of the ML-MotEx analysis of the XRD and PDF data of sample 1 (a-d), 2 (e, f) and 3 (g-j) respectively. Violin plot of the SHAP values obtained in the analysis of the different datasets, showing

preferable % *β*-MnO_2, P_b and P_r values and if intergrowth blocks in the starting model are favorable rather as a β- or R-MnO_2 block for the fit quality. (a, c, e, g, i) Each block in the supercell are colored with respect to the results from the ML-MotEx analysis. (b, d, f, h, j) If ML-MotEx prefer the block to be *R- MnO_2, it is colored blue, if ML-MotEx does not differentiate between the blocks, it is colored black and if ML-MotEx prefers β-MnO_2 it is colored red.*

Supplementary Notes 1: Whole Powder Pattern Modelling (WPPM)

Whole Powder Pattern Modelling is an approach for analysis XRD data based on modelling the experimental data bin one step developed by Scardi et al.[1] Instead of refining structural parameters by the mean of analytical functions such as pseudo-Voigt or Voigt, they model the XRD experimental pattern by convoluting the diffraction pattern of a crystalline phase by broadening models related to different effects, from the instrumental broadening of a peak to nanostructural effects such as finite size, strains or dislocations. Indeed, the diffracted intensity expressed as a function of the scattering vector s_{hkl} is a Fourier transform of the electronic density in a crystal. This analysis thus bases on the assumption that the contribution of each of the broadening effects listed before can be expressed as a sum of Fourier components that are added to the expression of the diffracted intensity. The analysis of Fourier components of these convolution functions allows a quantification of these different effects.

Following that type of methodology, it is possible to convolute the effect of a crystallite size distribution on the model. This size distribution must be modelled by a mathematical function and here we chose a lognormal distribution g(D) expressed as follow in Equation 6:

$$g(D) = \frac{1}{D\sigma\sqrt{2\pi}} e^{-\frac{(\ln D-\mu)^2}{2\sigma^2}} \qquad (6)$$

Where μ corresponds to the lognormal mean and σ corresponds to the lognormal variance. From these parameters μ and σ it is then possible to calculated the average size $D_{average}$ of the distribution and its standard deviation s.d. as shown on Equation 4 and 5:

$$D_{average} = e^{(\mu+\frac{\sigma^2}{2})} \text{ and } s.d. = (e^{2\mu+\sigma^2}(e^{\sigma^2}-1)) \qquad (4)\text{-}(5)$$

Some softwares are implemented with the WPPM method where the parameters related to the different contributions to the experimental XRD pattern are refined alongside unit cell parameters using a least-square method. Here we used PM2K, developed by Leoni et al.[2] In our case, we use WPPM to model the crystallite size distribution along the [100] direction of β- and R-MnO_2 domains in our samples by modelling the peak shape of the (110) peak of each parent structure. The fit of the peak performed on PM2K as well as the refined μ and σ values are shown in Fig S7. This yields a size distribution along the [110] direction. However, we want to determine it in the [100] direction. Assuming then that the finite size effect is the strongest along the [100] direction, i.e. the intergrowth direction, we then weight to yielded size distribution by a factor $(2)^{1/2}/2$ for β-MnO_2 domains as this corresponds to the ratio between the length of the [110] and [100] vectors in this structure, and by $(a^2+b^2)^{1/2}/a$ for R-MnO_2 as it corresponds to the same ratio in the R-MnO_2 structure. This allows to determine the Domains Size Distribution of R- and β-MnO_2 domains in our samples as shown in Fig 8.

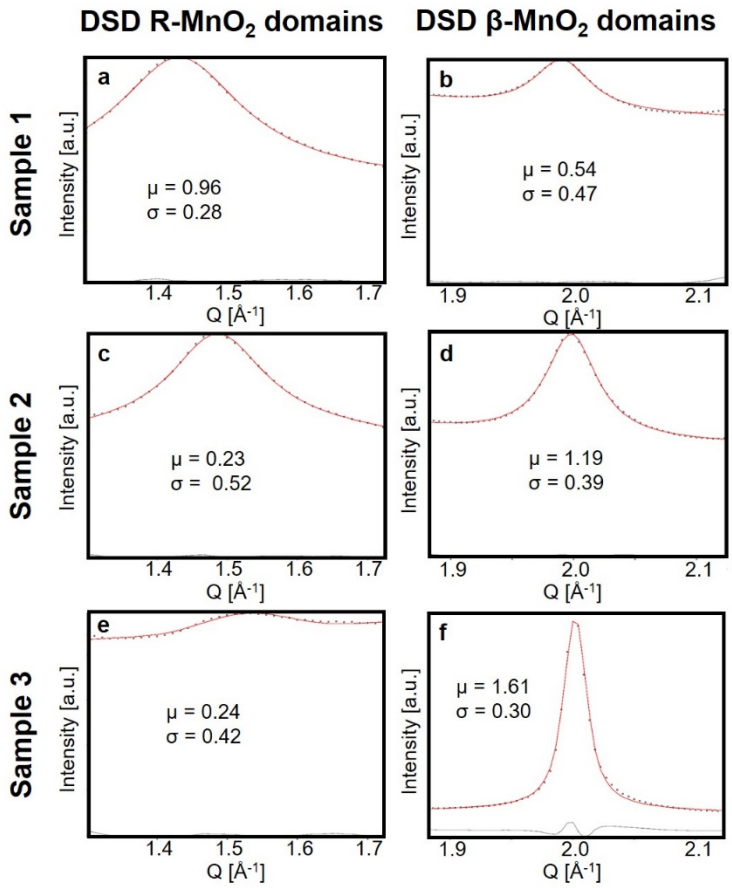

Figure S8: Fitting of the 110 reflection of R- and β-MnO_2 on XRD patterns of samples 1 (a-b), 2 (c-d) and 3 (e-f) by Whole Powder Pattern Modelling. The experimental data are represented by black dots, the calculated model in solid red line and difference curve in solid gray line.

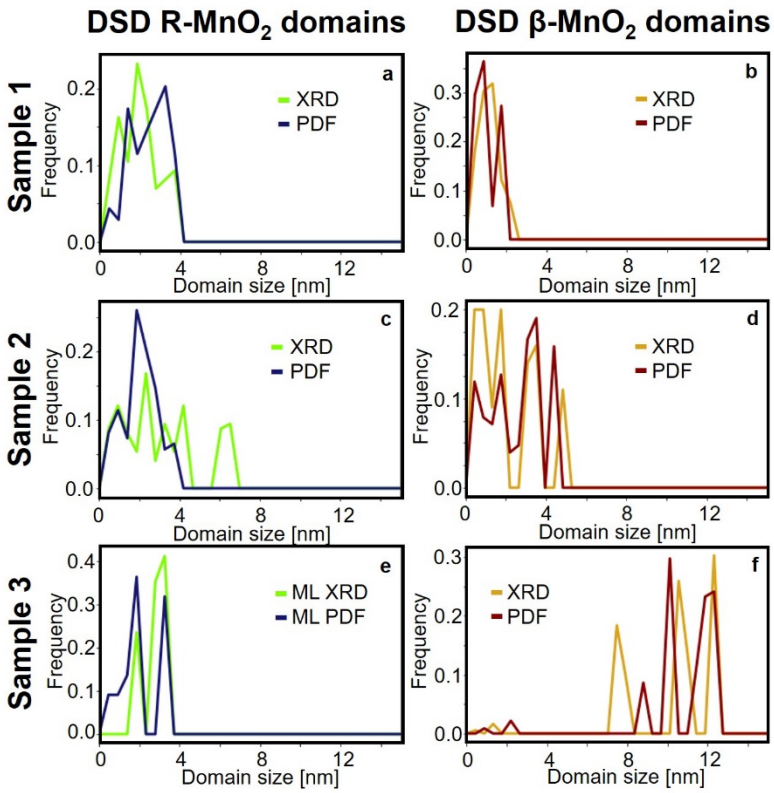

Figure S9: Calculated Domain Size Distribution of R- and β-MnO2 domains in supercells for which structure refinements are shown on Figure 6, i.e. supercells determined by peak-fitting method, for sample 1 (a-b), sample 2 (c-d) and sample 3 (e-f)

References:

1. Scardi, P.; Leoni, M., Whole powder pattern modelling. *Acta Crystallogr. A* **2002,** *58*, 190-200.
2. Leoni, M.; Confente, T.; Scardi, P., PM2K: a flexible program implementing Whole Powder Pattern Modelling. *Z. Kristallogr.* **2006**, 249-254.